Task 1 Report: Literature Review of Pile Driving System

Evaluation of Glass Fiber Reinforced Polymer (GFRP) Spirals in Corrosion Resistant Concrete Piles

FDOT Contract Number: BDV30 977-27, FSU Project ID: 042924

Progress report date: 4/12/2019

(Initial submission to FDOT Structures Research Center: 2/25/2019; First revision: 3/28/2019)

Submitted to:

Florida Department of Transportation

Research Center

605 Suwannee Street

Tallahassee, Florida 32399-0450

Christiana Freeman

Project Manager

FDOT Structures Research Center

FAMU-FSU Engineering

Prepared by:

Olayiwola Adegbulugbe

Graduate Research Assistant

Sungmoon Jung, Ph.D.

Principal Investigator

Raphael Kampmann, Ph.D.

Co-Principal Investigator

Department of Civil and Environmental Engineering
FAMU-FSU College of Engineering
2525 Pottsdamer St., Tallahassee, FL. 32310.

TABLE OF CONTENTS

LIST OF FIGURES

LIST OF TABLES

Chapter 1. Literature Review

1.1 Introduction

Concrete piles are installed into the ground using different pile driving systems. The operation and specifications of these driving systems are discussed in this chapter. Pile driving alters the characteristics of surrounding soil and causes local strains on the pile. It is therefore important to understand the interaction between a pile and the ambient soil characteristics: especially the soil stiffness and restraint of the pile during installation, as well as the dynamic response of the pile during impact driving activity. This chapter also reviews the specifications of the FDOT pendulum-impact facility as well as existing literature on the experimental apparatus to simulate concrete pile driving.

1.2 Pile Driving System

Factors such as soil properties, pile type, driving depth and installation procedure influence the magnitude of force needed to drive a pile to the desired depth. It is therefore imperative to select the most suitable and cost-effective equipment not only for a particular soil condition, but also for the pile material. The pile driving system also serves as a mechanism for evaluating the geotechnical resistance of piles.

Piles can be driven by a variety of hammers, each having its advantages and disadvantages. The project needs and the economy of the hammers also have to be considered before selecting a hammer. Generally, piles are driven either by impact or by vibration. Impact hammers are rated based on energy while vibratory hammers are rated based on power.

1.2.1 Impact Hammers

Impact hammers induce a downward velocity in the ram or drop weight to drive piles. When the ram impacts the pile, it produces a force sufficient to gradually advance the pile into the ground. Generally, impact hammers can be categorized as either external combustion or internal combustion. The power utilized by external combustion hammers is generated away from the hammer. External sources like the crane, air compressors, steam boilers and hydraulic power packs supply the energy required to move the ram upwards or downwards. Internal combustion hammers utilize the fuel within the hammer cylinder itself as the source of energy. An impact hammer produces a complete cycle of loading and unloading when driving a pile. The hammer produces a short duration force/velocity pulse in the driven pile. The duration of the impact itself is short compared to the duration between hammer blows during which the pile and the soil are at rest.

1.2.1.1 Drop (Gravity) Hammers

Drop hammers are the oldest type of pile driving hammer still in use. The ram or drop weight is raised by a crane mounted winch. When the winch brake is disengaged, the ram falls under its own weight to impact the pile. Energy is lost as the falling ram overcomes the rotational inertia of the winch cable (or hoist line). Hammer stroke is widely inconsistent and usually not well controlled. The ideal scenario is to engage the winch brake immediately after impact. However, if the brake is prematurely applied by the hammer operator in an attempt to prevent excessive spooling of the cable, the impact energy and efficiency of the hammer is reduced. The number of blows delivered per minute by a drop hammer is usually slow and dependent on the operator's experience and the fall height being used. These hammers should be operated carefully to avoid over-stressing and damaging the pile. Hence, the maximum stroke should be such that it does not damage the pile. Energy losses can be attributed to friction, inaccurate drop height, the rotational inertia of winch cable, premature application of brake and misalignment. Up to 50 % of the potential energy of the hammer can be lost (Rausche, 2000). These hammers are not very efficient compared to other hammer types. They are widely used for sheet pile installation where pile resistance is not a concern.

1.2.1.2 Air/Steam Hammers

These hammers operate using pressurized fluid (air or steam) within the hammer cylinder. Though originally developed to be powered by steam, majority of these hammers are now powered by compressed air. These hammers deliver constant stroke height on each blow once adjusted. They are of three varieties: single-acting, double-acting and differential- acting.

Figure 1.1 shows how a single-acting air/steam hammer works. The ram of single acting air hammer is connected to a piston on which the fluid acts. During the upstroke cycle, pressurized air or steam acts against the piston to push the ram upward. During the downstroke cycle, the valve controlling the fluid is closed, and the ram falls freely for impact delivery. Pressure enters the cylinder again as the pressure valve is activated shortly before impact to begin a new cycle. The efficiency of these hammers is assumed to be 67 % for wave equation analyses (Rausche, 2000). However, because the hammer can overstroke on the short stroke hammer efficiency can be increased for wave equation analysis. Energy transfer efficiency at the end of driving is an average of 55 % for steel piles and 40 % for concrete and timber piles (Rausche, 2000).

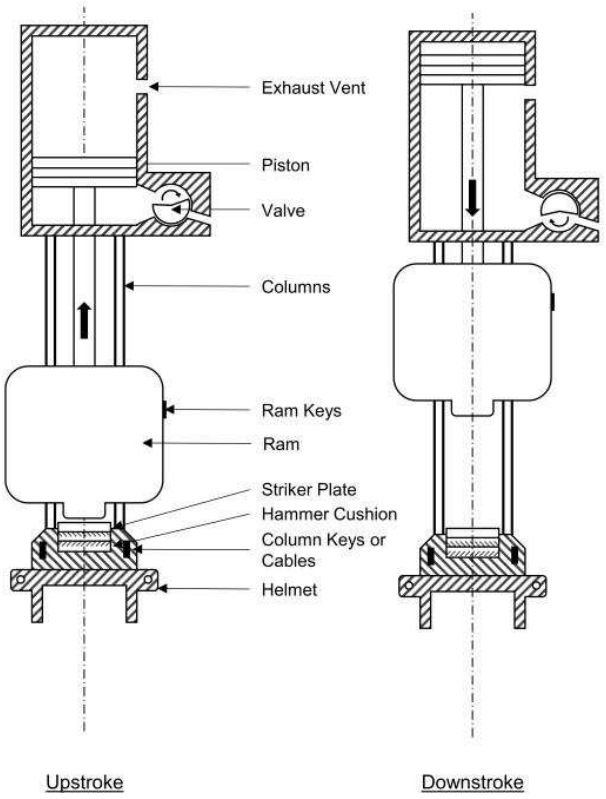

Figure 1.1: Operation of a Single-acting Air/Steam Hammer (Hannigan et al., 2016b)

The weights of these hammers are usually higher than the weights of drop hammers. Single-acting air/steam hammers are relatively simple to operate and are not very expensive. Many pile types can be driven using this hammer: especially large steel and concrete piles, and are usable in all soil conditions, particularly in heavy clay. They however cannot be used as extractors.

Double-acting air/steam hammers are similar to single acting air/steam hammers. However, when the fluid raises the ram and the valve is tripped in double acting air/steam hammers, fluid is also applied to the top of the piston to provide downward active pressure, thereby forcing out the fluid below the piston. As a result, the stroke is shorter and these hammers operate at more than twice the speed of single-acting air/steam hammers. This results in a higher blow rate even with the same ram weight as the single acting hammer. Although they are able to deliver more blows per minute than single acting air/steam hammers, they rely heavily on air pressure and have been historically observed to be slightly less efficient in comparison to equivalently rated single hammers.

Differential-acting air/steam hammers have two pistons that are constructed such that the top surface of the upper piston is larger than the top surface of the lower piston. When the valve is tripped, pressure is applied to the two pistons which are connected to the ram. The top chamber of the hammer cylinder is

under atmospheric pressure only, while motive fluid is applied in the bottom chamber. The difference in the area of the pistons ensures that the pressurized fluid between the pistons produces a net upward force for upstroke. For downstroke, the ram is forced down with a velocity higher than free fall and the fluid below the piston flows to the top of the piston as it falls. Also, these hammers operate at half the stroke and twice the speed of single-acting hammers. Differential-acting air/steam hammers have lower efficiency compared to equivalent single acting air/steam hammers.

For the final bearing of piles driven by air-steam hammers to be acceptable, the hammer must operate within 10 % of the manufacturer's rated speed, unless otherwise stated (Florida Department of Transportation, 2015).

1.2.1.3 Hydraulic Hammers

Hydraulic fluid under pressure from an external power pack is applied to the piston to set the ram in motion. They can be single acting or double acting.

In single-acting hydraulic hammers, pressurized fluid raises the ram to a predetermined height, then the ram is allowed to fall freely or as freely as the escaping fluid permits. After impact, the ram is raised again by the hydraulic system to begin a new cycle. Figure 1.2 shows a diagram of a single acting hydraulic hammer.

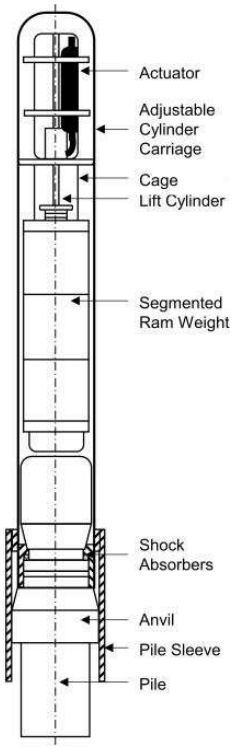

Figure 1.2: Schematic of a Single-acting Hydraulic Hammer (Hannigan et al., 2016b)

A pendant on the hydraulic power pack controls the volume of fluid supplied to raise the ram. The pendant controls and continuously adjusts the stroke and blow rate of the hydraulic hammer. The hammer short stroke can be set to as small as 6 inches to prevent pile run during easy driving. Hard driving can be achieved at higher strokes. The stroke can be visually estimated on several single acting hydraulic hammers. In newer single acting hydraulic hammers the ram velocity just before impact can be observed from an inbuilt monitoring system. The stroke and kinetic energy of the hammer can be calculated from the measured ram velocity.

1.2.2 Diesel Hammers

These hammers are the only internal combustion hammers of the impact hammer group. The energy required to drive the hammer comes from the combustion of diesel within the combustion chamber of the hammer. Diesel hammers are classified as either open-end or closed- end.

In open-end (single-acting) diesel hammers, a starting device or hoist initially lifts the ram upward, and then the ram is then released and allowed to fall under gravity. As it passes the exhaust port located on the side of the hammer cylinder, air trapped in the lower part of the cylinder is compressed. Before the bottom of the ram passes through the exhaust port, the piston pushes the fuel pump or injector fuel, and fuel is sprayed into compressed air within the cylinder. At the end of the downstroke, the initial volume of air becomes compressed to a very small volume. Once the ram strikes the anvil, the increased pressure coupled with a rise in temperature creates combustion that subsequently thrusts the ram upward and transmits driving impulse to the pile. Spent gases exit the system as the ram passes the exhaust port during upstroke. This cycle continues repeatedly until fuel is no longer supplied. Figure 1.3 shows the operation of an open-end diesel hammer.

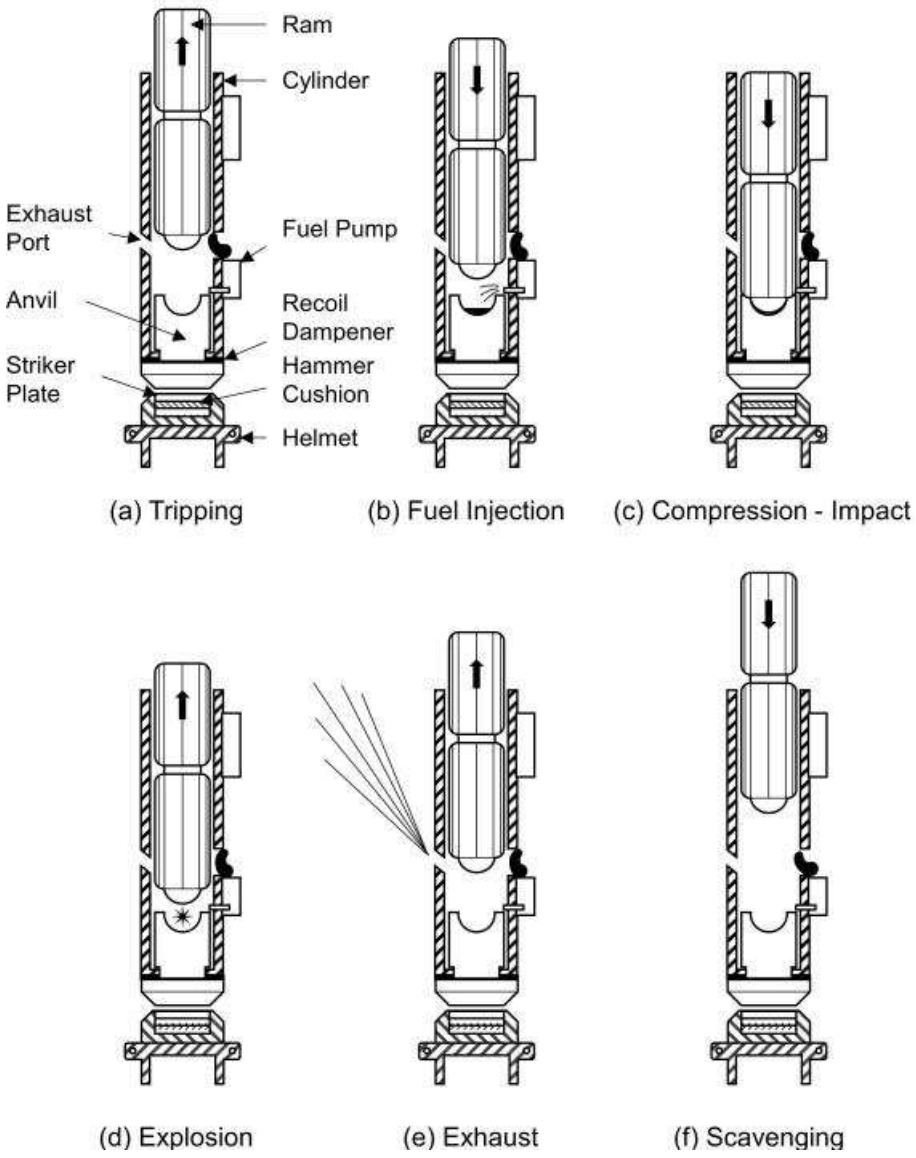

Figure 1.3: Operation of an Open-end Diesel Hammer (Hannigan et al., 2016b)

Closed-end (double-acting) diesel hammers have a closed cylinder top that distinguishes them from open-end diesel hammers. The starting operation is also the same as with the open-end hammers. During upstroke, air is compressed at the upper part of the hammer cylinder, known as the bounce chamber (or compression chamber). The compressed air within the bounce chamber shortens the ram stroke and increases the blow rate. Pressurized air exit the bounce chamber via the bounce chamber port during downstroke.

1.2.3 Vibratory Hammers

Vibratory hammers operate by applying a rapidly alternating force powered hydraulic power packs to drive piles into the ground. They have pairs of hydraulic motors with counter rotating eccentric weights.

Two eccentric motors act such that their axial force components add up while their lateral centrifugal force components cancel each other, therefore eliminating lateral whip. The vibratory mechanism therefore produces a sinusoidal axial force with a frequency equal to the speed of the rotating motors. Vibratory machines can also have multiple pairs of smaller, identical eccentrics that produce the same results as a large pair. The maximum downward dynamic force produced is given by

$$F_F = (2\pi f)^2 M_E \qquad (1.1)$$

where:

F_F = dynamic force

f = hammer frequency

M_E = summation of all eccentric moments

Hydraulically activated clamps connect the hammer with the pile and static weights added above and isolated from the vibrators give the hammer sufficient mass for driving. To advance the piles, these hammers operate at a frequency that excites the soil and vibrates it out of the way ensuring that pile penetrates under self-weight and the weight of the hammer. Vibratory hammers are not rated by impact energy delivered per blow, they are rather rated on the frequency of energy developed per second and/or by the force delivered to the pile by the hammer. To accept piles from a bearing perspective, a blow count criterion will be required, as a result, an impact hammer will be required at the end of the driving to obtain the bearing capacity of the pile. These hammers are usually powered by a hydraulic power pack. Vibratory hammers are not suitable for installing prestressed concrete piles due to tensile and bending stress which can damage the piles. Applications of these hammers include: driving and extracting sheet piles and installation of non-displacement piles. Difficulty in laterally displacing the soil at the pile toe makes this hammer less suited for installing closed-end pipes and other displacement piles. Vibratory hammers can work in silt or soft clays. However, they work best in granular soils, especially in submerged conditions. They are not recommended for stiff to hard clays.

1.2.4 Resonant Hammers

Resonant hammers are essentially vibratory hammers that operate at even higher frequencies. These hammers advance piles by using high frequency vibration generated by a hydraulic piston-cylinder to induce resonance responses in piles. A valve controlling the supply of hydraulic oil to alternating sides of the piston adjusts the amplitude and magnitude of the oscillating force generated by the hammer. Operating frequencies of up to 180 Hz can be reached. Driving piles with these hammers require that the

frequency range of the machine be properly matched with the length of the pile. Resonant hammers cannot be used in determining the bearing capacity of a pile. Hence, a conventional impact hammer must be used after installation with the resonant hammer is complete.

1.3 Hammer Energy

Hammers that operate based on the gravity only are rated by their potential energy at full stroke, i.e., the product of the ram weight and the stroke. These hammers include drop, single acting air/steam, single acting hydraulic and open-end diesel hammers. Other hammers however can be rated by other principles of energy rating depending on the manufacturer. For double-acting hammers, the equivalent stroke is increased due to increased pressure than free fall, thereby reducing the duration of every blow cycle. The equivalent stroke of double acting hammers is the stroke of the corresponding single-acting hammer that produces the same impact velocity. Table 1.1 shows the range of the energy, impact velocity and blow rates of different hammer types. The rated energy, ram weight and stroke of different types of hammers from different manufacturers can be found from Hannigan et al. (2016a).

Equation 1.2 shows the impact velocity, V_i, calculated from the maximum stroke.

$$V_i = (2gh)^{1/2} \qquad (1.2)$$

where

V_i= impact velocity, *ft/s*

g = acceleration due to gravity, *ft/s*^{2}

h = ram stroke, *ft*

The kinetic energy from the hammers is less than the potential energy because energy is lost to friction, misalignment, residual fluid pressure, preignition, etc. Additional energy is lost to the hammer cushion, helmet, pile cushion and inelastic collision at the pile head. The kinetic energy is computed as shown in equation 1.3 below.

$$\text{KE} = \frac{1}{2} m V_i^2 \qquad (1.3)$$

where

KE = kinetic energy

m = ram mass

V_i = impact velocity

Energy transferred to the pile top is calculated as shown in equation 1.4.

$$\mathrm{E(t)} = \int_0^t F(t)v(t)dt \qquad (1.4)$$

where

$\mathrm{E(t)}$ = transferred energy

$F(t)$ = average pile force

$v(t)$ = velocity

Table 1.1: Pile Hammer Characteristics

Hammer Type	Rated Energy (ft-kips)	Impact Velocity (ft/sec)	Blow Rate (blows/minute)	Energy (per blow)
Drop (Gravity) Hammers	7 to 60	23 to 33	4 to 8	Ram weight x height of fall
Single Acting Air/Steam Hammers	7 to 1800	8 to 16.5	35 to 60	Ram weight x height of fall
Double Acting Air/Steam Hammers	1 to 21	15 to 20	95 to 300	(Ram weight + effective piston head area x effective fluid pressure) x stroke
Differential Acting Air/Steam Hammers	15 to 50	13 to 15	98 to 300	(Ram weight + effective piston head area x effective fluid pressure) x stroke
Single Acting Hydraulic Hammers	25 to 2162	5 to 18	30 to 50	Ram weight x height of fall
Double Acting Hydraulic Hammers	25 to 2581	5 to 23	40 to 90	(Ram weight + effective piston head area x effective fluid pressure) x stroke
Open-end Diesel Hammers	9 to 1620	10 to 16.5	40 to 60	Ram weight x height of fall
Closed-end Diesel Hammers	5 to 73	8 to 16.5	80 to 105	(Ram weight + effective piston head area x effective fluid pressure) x stroke
Vibratory Hammers	—	—	750 to 2400	—

			vibrations/minute	
Resonant Hammers	—	—	up to 10,800 vibrations/minute	—

1.4 Soil Resistance

The installation of a pile severely distorts the soil surrounding the pile. To successfully drive a pile the resistance of the hammer-pile-soil system should overcome the resistance of the soil. The resistance exerted by soil on a pile during installation can be divided into side friction, which is distributed along the pile shaft, and end bearing, which acts at the toe of the pile. The area of pile considered in side friction depends on the embedded pile length, whereas end bearing resistance utilizes the cross section of the pile as the effective gross area (Guades et al., 2012). Equation 1.5 shows the total (ultimate) capacity Q_{total} of a pile as the sum of the side friction resistance Q_{sL} and the end bearing resistance Q_b.

$$Q_{total} = Q_{sL} + Q_b \tag{1.5}$$

$$Q_{sL} = \sum_{i=1}^{n} q_{sLi} A_{si} \tag{1.6}$$

$$Q_b = q_b A_b \tag{1.7}$$

where:

q_{sLi} = Unit shaft resistance for each soil layer

A_{si} = Pile shaft area interfacing with layer i

q_b = Unit base resistance

A_b = Area of pile base

In saturated cohesive soils, driven piles generate strain fields (zone of disturbance) close to the toe of the pile and along the shaft of the pile. The soil in the vicinity of the pile is radially compressed outwards. During installation, high (positive) pore water pressure exists around the shaft due to increased stresses as the soil is radially compressed outwards to accommodate the pile volume. This in turn temporarily reduces the shear strength and resistance of the soil, and subsequently the blow count or pile penetration resistance. After the installation of a driven pile, the cohesive soil around the pile begins to reconsolidate immediately as high pore water pressure dissipates radially. As a result, the shear strength of the soil, as

well as the pile resistance, increases along the toe and shaft of the pile. This phenomenon is referred to as "setup". A significant increase in side shear strength has been observed in cohesive soils within the first 24 hours after pile installation (Bullock et al., 2005). The rate of side shear increment reduces with time. Researchers have proven through static and dynamic tests that side shear other than end bearing resistance contribute mostly to the setup (Bullock et al., 2005; Bullock, 2008). More shear strain and disturbance occurs along the shaft of the pile than at the toe, given a larger contact area on the side versus the toe. Therefore, soil reconsolidation and dissipation of the high pore pressure generates significant side shear strength. Driven piles in partially saturated soils do not experience significant setup since high pore water pressure was not generated.

During the installation of a pile, the relative density of loose to medium dense noncohesive soil around the pile is increased as a result of the lateral displacement of the soil. Increased relative density increases resistance of the pile. In dense cohesionless soils, pile installation may decrease the relative density of the soil, since the soil dilates during shear and displacement (Herrera et al., 2018). This may result in a temporal negative pore pressure, which in turn temporarily increases the resistance along the pile shaft and below the pile toe. After installation, the built-up stress is reduced as the pore pressure generated initially is dissipated. This phenomenon is referred to as "relaxation" as explained by Equation 1.8 for soil shear strength. The expression $(\sigma - u)\tan\phi$ changes to $(\sigma + u)\tan\phi$ during the temporal negative pore pressure. As the negative pore pressure dissipates, the shear strength and resistance along the shaft and below the pile toe decrease.

$$c + (\sigma - u)\tan\phi \qquad (1.8)$$

where:

τ = Shear strength of soil.

c = Cohesion.

σ = Total normal stress (pressure) on plane of failure.

u = Pore water pressure.

ϕ = Angle of internal friction.

"Setup" as described above can also occur in saturated noncohesive silts and loose to medium dense fine sands. However, setup happens faster in sands and silts than in clays because pore pressure is dissipated

quicker in noncohesive soils than in cohesive soils. However, according to Bullock et al. (2005), less overall setup occurs in noncohesive soils.

Dynamic and static tests performed on 457 mm (18 in) square prestressed concrete piles on four Florida bridge sites (Buckman Bridge, Aucilla River Bridge, Vilano Bridge and Seabreeze Bridge) were reported by Bullock (1999) and Bullock et al. (2005). These sites were chosen to obtain results for different soil types – sand, clay and mixed soil. Osterberg cell tests were used to separate side friction and end bearing resistance. Table 1.2 provides information on the nature of the soil, the length of tested piles and penetration of tested piles for each bridge site. It also shows the side and end bearing resistance of the piles reported at the end of driving. Higher values of side friction resistance were reported after restriking each pile.

Table 1.2: Summary of pile tests by Bullock et al. (2005)

Bridge site	Nature of soil	Pile length (m)	Pile penetration (m)	End bearing resistance (kN)	Side friction resistance (kN)
Buckman Bridge, Jacksonville, FL	Dense fine sand	10.05	9.16	1837	0
Aucilla River Bridge, Aucilla, FL	Soft to medium stiff silty clay and Fine sand	21.33	19.19	1200	188
Vilano Bridge East AIA, Vilano Beach, FL	Dense fine sand	11.88	10.68	1900	773
Vilano Bridge West AIA, Vilano Beach, FL	Soft to medium stiff silty clay	19.96	18.40	540	5
Seabreeze Bridge, Daytona Beach, FL	Medium to fine sand and silty clay	26.84	25.12	1000	470

1.5 Dynamic Response of Piles during Installation

Piles are inspected by static load test and dynamic test methods. Static load testing requires a large surcharge load, is time consuming and usually only applicable to a limited number of piles. Dynamic tests, on the other hand, are cheaper, reliable, can be performed within a short time and provides increased quality control (Likins, 1984; Ding et al., 2011). There are two methods of dynamic testing: low strain (impact-echo) and high strain testing. The dynamic testing described below belongs to the high strain dynamic test category.

Dynamic pile testing helps to investigate the relationship between the surrounding soil and a driven pile during or after installation. Early researchers estimated pile capacity from blow counts, which now is considered unreliable (Likins et al., 2000). The one-dimensional wave equation analysis program (WEAP) was developed to analyze and process test data from the field. It provided a realistic approach in modeling the hammer, driving system, pile and soil, as well as simulating the pile driving process (Rausche, 2000; Bullock, 2012). In one-dimensional wave equation analysis, the pile capacity can be estimated using the hammer energy transfer, the permanent set per blow, soil damping, etc. WEAP however requires assumptions due to the limited information on the soil and hammer parameters. Modern dynamic testing of piles is based on measurements from a Pile Driving Analyzer (PDA). The PDA test is a popular dynamic test procedure for evaluating the bearing capacity, driving stresses, hammer performance and integrity of driven piles during initial driving and restriking. Hammer impact on a pile produces strain and acceleration which are measured by the strain gages and accelerometers mounted close to the pile head. Data acquired from these sensors are transferred via a cable to the PDA (Figure 1.4) which processes the data to display a plot of force and velocity. Penetration resistance is another vital and separate component of the dynamic test required to analyze pile capacity.

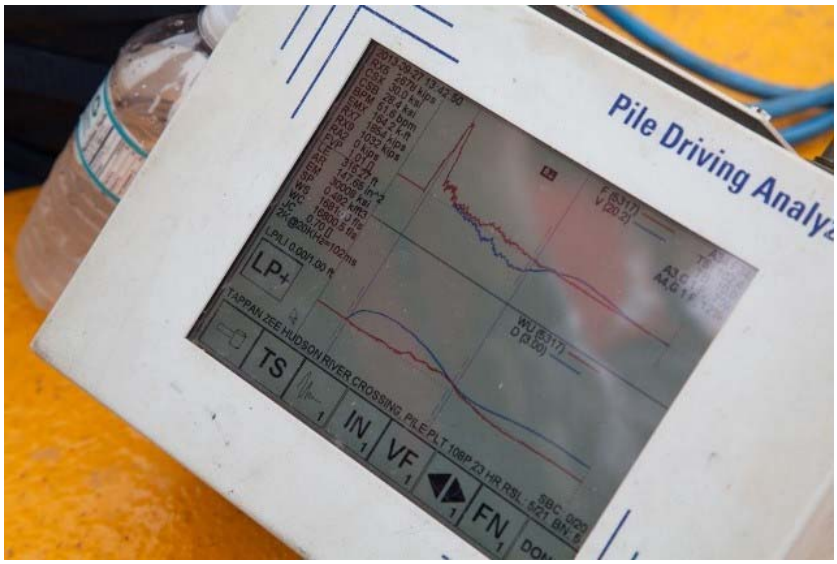

Figure 1.4: Pile Driving Analyzer (PDA).

The dynamic response of the pile due to a suddenly applied axial load can be explained using the propagation of a stress wave (Clough and Penzien, 1993). In order to explain amplification of the stress at the pile toe, suppose that the magnitude of the impact is P_0 and the pile toe has fixed boundary condition. After the impact at the pile top, a force wave of amplitude P_0 travels downward. Reflection of this force wave at the toe, according to the wave propagation theory, causes the force wave to be doubled near the

rigid support. On the other hand, reflection of the wave at the pile top (free end) is a negative reflection causing a reduction of the force. The force in the pile is related to the particle velocity as follows.

$$\mathrm{F} = Zv \qquad (1.9)$$

where:

F = Force in the pile

v = Particle velocity

Z = Pile impedance given by equation 1.10

The impedance of the pile dictates the amount of hammer energy transmitted `through the pile into the soil. The greater the impedance of the pile the greater the energy transmitted through the pile into the soil (Ashford and Jakrapiyanun, 2001; Guades et al., 2012)

$$Z = \frac{EA}{c} = \rho Ac \qquad (1.10)$$

where:

E = Elastic modulus of pile

A = Cross sectional area of pile

c = Wave speed given by equation 1.11

ρ = mass density of pile material

$$c = \sqrt{\frac{E}{\rho}} \qquad (1.11)$$

Also, c can be determined from the time ($2L/c$) taken by the wave to travel up and down the pile length, L.

The wave force-velocity plot provides a visual indication of the dynamic and static resistance. Dynamic resistance is a function of pile velocity, and the static resistance depends on the movement, required to mobilize the ultimate static resistance. The static resistance of a pile can be obtained by subtracting the dynamic component, expressed as the product of a selected damping factor and the pile toes velocity, from the total resistance (Bullock, 2012). The pile capacity obtained from a dynamic test corresponds to

properties of the pile-soil system only at the time of testing. The real-time data processing from the PDA produces results for evaluating hammer performance, compression and tension stresses during pile driving, pile structural integrity, distribution of soil resistance and the static load-bearing capacity of the pile (Hussein and Goble, 2004; Hussein et al., 2006).

The maximum allowed pile stresses are given in the Florida DOT Standard Specifications 455-5.12.2 (FDOT, 2018). During pile driving, the compressive tensile stresses should not exceed the Specification limits. Care should be taken (ex: reduced stroke) when driving the pile into weak soils to control the tensile stress. The primary focus of this project is to design the spiral to support the compressive stress during the driving. The maximum allowed pile compressive stress (psi) for concrete pile is given as:

$$s_{apc} = 0.7f_c' - 0.75f_{pe} \qquad (1.12)$$

where:

f_c' = specified minimum compressive strength of concrete (psi)

f_{pe}= effective prestress (after all losses) at the time of driving (psi), taken as 0.8 times the initial prestress force.

Roddenberry et al. (2014) drove two 24 in. square CFRP prestressed concrete piles as part of the Deer Crossing Bridge project. The stress measurement during the pile installation (CSX: maximum measured average stress) reached up to 4.0 ksi. The report compared the stress measurement with the s_{apc} from Equation (1.12) as follows (p. 80 and pp. 239-240). Based on the measured compressive strength $f_c' = 10000$ and design $f_{pe} = 1000$, the measured stress did not exceed $s_{apc} = 6.25$ ksi. On the other hand, based on the typical limit in production pile using the assumption of $f_c' = 6000$ and $f_{pe} = 800$, the measured stress was greater than $s_{apc} = 3.6$ ksi.

Post-testing analysis of the data obtained from the PDA can be conducted using a signal matching computer algorithm known as the Case Pile Wave Analysis Program (CAPWAP), which extracts the soil parameters active during impact from PDA measurements, accepts the downward wave as input and iteratively estimates the resistance model to calculate the upward wave. The calculated upward wave can be used to validate the measured upward wave. Results obtained from CAPWAP include static resistance along the pile shaft (or skin friction), static resistance at the pile toe (end bearing), soil quake and damping values in friction and end bearing as well as a simulated static load versus movement graph (Rausche et al., 1994; Hussein et al., 2006; Rausche et al., 2010; Bullock, 2012).

More recently, McVay et al. (2002) in collaboration with FDOT developed a system that includes instrumentation embedded in the pile. The goal is to provide an alternative method of calculating real-time static resistance by using damping values obtained in real-time during pile driving.

The system consists of accelerometers and strain transducers near both ends of the pile (pile top and tip). An antenna which is connected to the embedded instrumentation is located at the face of the pile. A field receiver collects and analyzes data transmitted from the antenna to provide real-time estimates of static capacity, pile stresses and energy transferred to the pile for every hammer blow, thereby providing the information needed for evaluating the driving system and soil resistance (Herrera et al., 2009). According to Herrera et al. (2009), the total static resistance estimates from this method are on the average within 15% of the PDA-CAPWAP estimates.

1.6 FDOT Impact Pendulum Test Facility

The pendulum-impact facility at the Florida Department of Transportation (FDOT) Marcus H. Ansley Structures Research Center in Tallahassee, Florida, comprises of three free standing 50 ft galvanized pylons (steel towers) and a heavily reinforced concrete foundation for the anchor system. The pylons are each supported on a drilled shaft foundation that is 19 ft long with a diameter of 4 ft. The elements of each pylon include three 12 in. diameter steel piles with several L5×5×5/16 steel angles (Consolazio et al., 2012). The drop height of the pendulum mass is adjusted by a steel cable, pulley and winch system on one of the pylons, while the other two pylons have four cables between them that support the swing of the pendulum mass during operation. The pendulum support structure has the capacity to swing an impact mass of up to 9020 lbs. (4090 kg) through a drop height of 35 ft. The FDOT pendulum can deliver impact energies up to approximately 315 kip-ft (427 kJ). The length, width and depth of the reinforced concrete foundation for the anchor system are 34 ft, 20 ft and 3 ft respectively. See Figure 1.5.

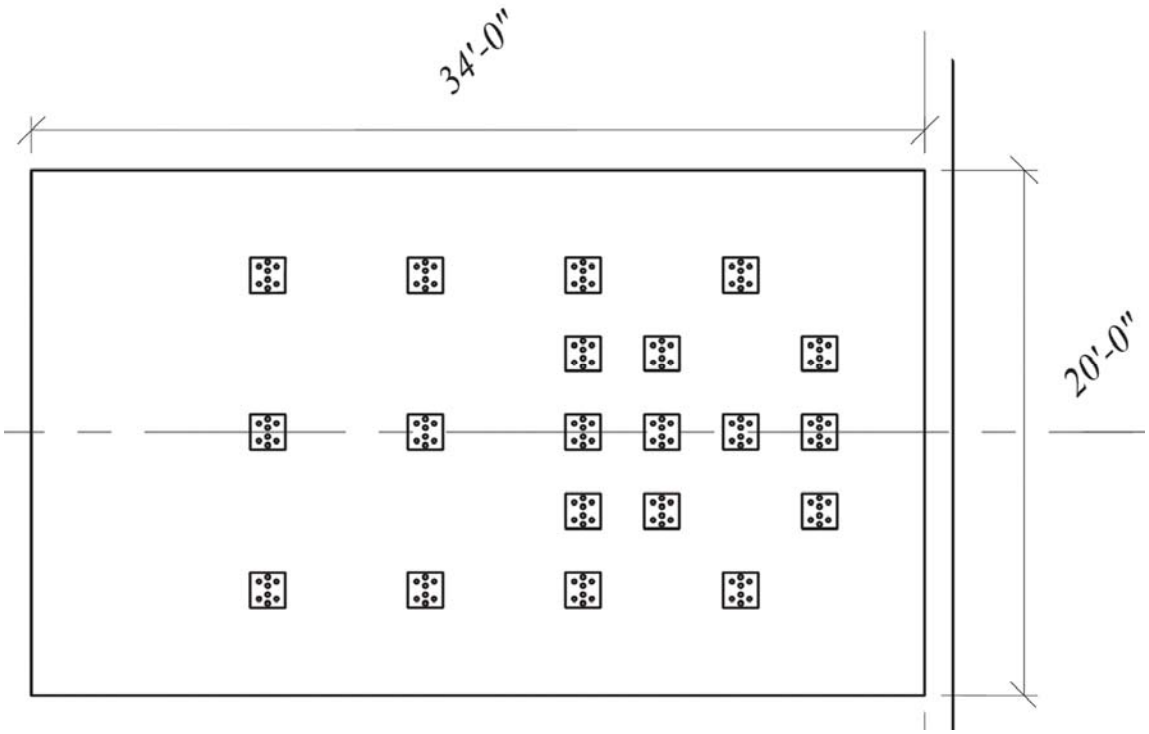

Figure 1.5: Reinforced concrete foundation and anchors in FDOT pendulum facility (Consolazio et al., 2014)

Three surface-mounted accelerometers are typically employed on the impact mass to record the time-varying deceleration: two accelerometers in the direction of impact and a third in the vertical direction (Kantrales et al., 2015). Data from these accelerometers serves as a basis to quantify the time-varying impact force.

1.7 Experimental Apparatus to Simulate Pile Driving

McVay et al. (2015) conducted experiments to investigate the pile wave propagation of typical FDOT full-scale piles with and without soil. In the experiment conducted without soil, an 18 in. × 18 in. × 180 in. pile with EDC near the top and bottom was supported by 6 ft long cargo straps. The straps were suspended by two steel frames. A cylindrical steel pipe hammer, with dimensions 2 ft, 3 ft and 0.5 in. corresponding to the inner diameter, length and thickness of the steel pipe was filled with concrete. The hammer weighed 1000 lbs. and was suspended from a 28 ft tall forklift frame. Figure 1.6 shows the schematic of the experimental setup. To apply blows to the pile, the hammer was pulled backward till it reached the required vertical height and then allowed to fall freely. In addition to the EDC, the test pile was instrumented with PDA accelerometer and strain gages, as well as the UF accelerometer and strain gages.

The test conducted to investigate soil-pile interaction utilized the same cross-sectional dimensions, but the length of the pile was 30 ft. The pile was placed horizontally in a 150 cubic yard Florida silty-sand soil. The soil had a moisture content of 11 % and a dry unit weight of 110 pcf before being placed, and these parameters were intermittently checked again while the soil was placed. The soil was compacted using walk-behind compactors. 20 ft of the pile length was buried into the compacted soil. Again, the embedded pile was instrumented with EDC near the top and bottom of the pile. Also, the pile was instrumented externally using piezo-resistant accelerometers at the bottom of the pile, and piezo-electric accelerometers at the top of the pile. The same hammer as described above was used to impact the pile. The hammer was suspended as a pendulum by a 20 ft steel channel connected to a large forklift. The strike distance of the hammer was controlled between 4 ft to 6 ft chord length, equivalent to a drop height of 1 ft, and 14 ft to 16 ft chord length, equivalent to a drop height of 6 ft.

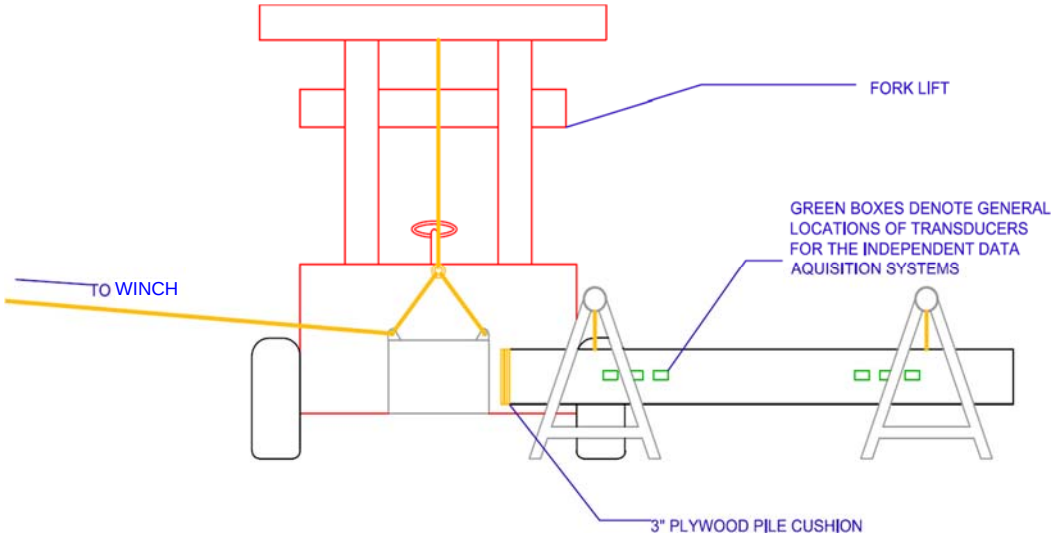

Figure 1.6: Pile Driving Apparatus (McVay et al., 2015).

McVay et al. (1994) developed a novel centrifuge modeling apparatus for driving scaled model piles in a laboratory setting. Also, the apparatus was not only capable of driving and laterally loading groups of six to nine model piles but does so while the centrifuge is in flight. The apparatus which is connected to a computer, consists of a soil container, a top beam attached the pile driving mechanism, and a pile driving sequencer plate among many features described by the author. Pile driving is initiated by the computer signal, lateral load is provided by a 1200 lbs. air cylinder (R) as shown in Figure 1.7. A 0.25 in. range LVDT was employed to measure the lateral movement. The computer which was also equipped with a software, controlled (raised and lowered) the pile driving mechanism, drove each pile and recorded the results.

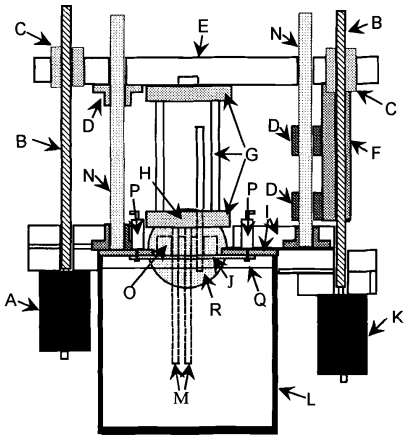

A. STEPPING MOTOR (LEFT)
B. BALL SCREW
C. BALL NUT
D. PILLOW BLOCK BEARING
E. TOP BEAM
F. SIDE BEAM
G. PILE DRIVING APPARATUS
H. PILE DRIVING SEQUENCER
I. BASE BEAM
J. PILE CAP SUPPORT "TRAP DOOR"
K. STEPPING MOTOR (RIGHT)
L. SOIL CONTAINER
M. MODEL PILES
N. STEEL GUIDE ROD
O. PILE CAP
P. AIR PISTON FOR TRAP DOOR
Q. SOIL SURFACE
R. AIR PISTON FOR LATERAL LOAD

Figure 1.7: Centrifuge Pile Driving Apparatus (McVay et al., 1994).

Model piles were made of high strength aluminum tubing that was 11 inches in length from the bottom of the pile cap and had an outer and inner diameter of 0.375 in. and 0.305 in. respectively. This simulated open-ended piles that had a diameter of 18 in., a length of 44 ft and a flexural stiffness (*EI*) of 28.98 × 10^8 lbs. $in.^2$. Pile models were driven at 48 times the normal gravitational field (48 g). The author conducted the experiment using the Reid-Bedford sand because the research was concerned with ship impacts in Florida and 90 % of usable waterways in Florida are on sand or silty sand. Also, the properties of the selected soil were widely published. The Reid-Bedford sand is a fine, brown, subrounded to subgranular material. Its composition is 89 % quartz, 9 % feldspar and 2 % ferromagnesium. It has unit weights ranging from 86.5 lb/ft^3 (13.59 kN/m^3) to 106.5 lb/ft^3 (16.74 kN/m^3). Reid-Bedford sand samples utilized for the experiment had a friction angle of 31° and 38° depending on their unit weights.

McVay et al. (2000) in another example of a centrifugal test investigated the influence of pile caps at large deflections. Four different locations of the pile caps were considered in this study. The centrifuge utilized in this research had a payload capacity of 12.5 g- tons. The specimen platform is 1.6 m away from the center of rotation. To stimulate field stress conditions, the model piles were driven in flight at 45 g. Lateral load was applied to model pile groups by an air piston with a pressure rating of 125 psi. The piston could supply a maximum lateral load of 1200 lbs. which is equivalent to a real load of 1215 tons. Lateral displacements were measured using an LVDT. The model piles were made of solid square aluminum (6061 alloy) bars and had a width of 3/8 in. and lengths of 11.54 in., 9.53 in., 8.50 in. and 7.52 in. equivalent to 17-inch prototype width and prototype lengths of 43.31 ft, 35.76 ft, 31.82 ft and 28.22 ft.

Sand gotten from the sand mine in Edgar, Florida, which had a mix of different gradation was utilized for the test. The gradation of the sand mixture was close to that of the Reid-Bedford sand. Further details about the apparatus (Figure 1.8) were also described by McVay et al. (1998).

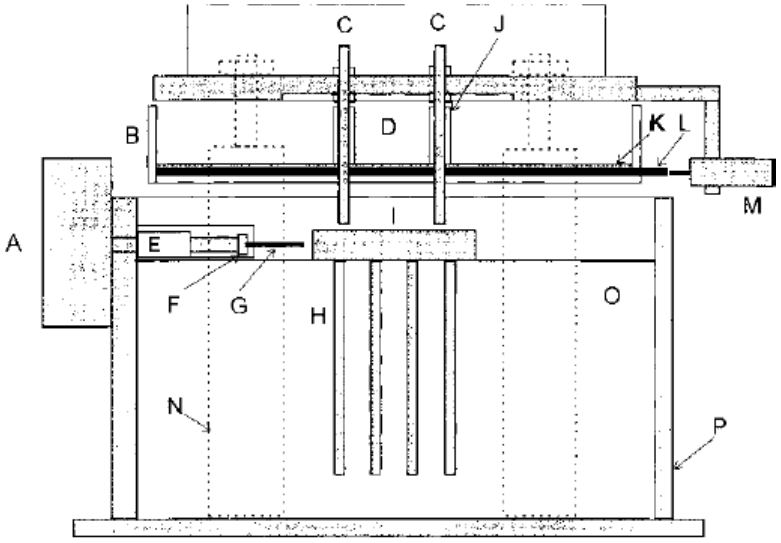

A. Lateral load piston
B. Sand hopper box
C. Driving rod
D. Sand to be rained
E. Pillow bearing
F. Load cell
G. Loading rod
H. Piles
I. Pile cap
J. Protection tube
K. Stationary plate
L. Movable plate
M. Piston for sand raining
N. Master driving pistons
O. Foundation sand
P. Model container

Figure 1.8: Centrifuge Pile Driving Apparatus (McVay et al., 2000).

El-Garhy et al. (2013) performed model tests on a single pile, unpiled rafts and central piled rafts. Soil used in the experiment was classified as poorly graded dry sand. The sand had a unit weight of 15.5 kN/m^3 and an angle of friction of 33°. Model piles (Figure 1.9) used were steel hollow piles with an outer diameter of 10 mm and a thickness of 1.5 mm. Pile length used were 200 mm, 300 mm and 500 mm. The modulus of elasticity of the steel pipe used was 2.1×10^8 kPa. A pile shoe was fixed to the pile tip while the pile head had a bolt that provided a connection with the pile cap. The soil was placed in a steel tank had a depth of 1 m, a length of 1 m and a width of 1 m. Loads were applied by a hydraulic jack connected to the top of a steel frame over the tank as shown in Figure 1.10.

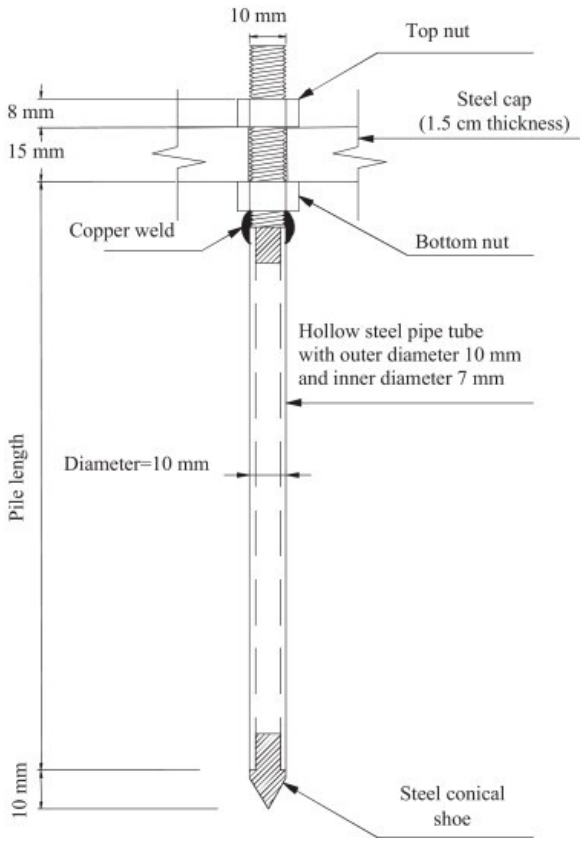

Figure 1.9: Model Pile (El-Garhy et al., 2013).

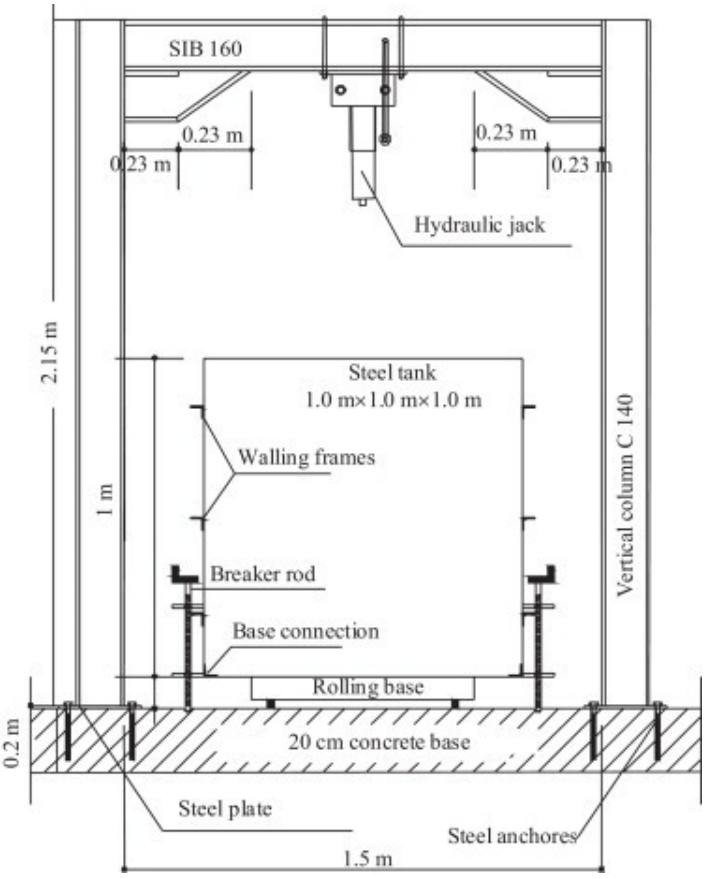

Figure 1.10: Vertical Cross Section of Apparatus (El-Garhy et al., 2013).

1.8 Field Pile Testing

Fam et al. (2003) performed full-scale field testing on a conventional square prestressed concrete pile and a circular precast composite pile. Figure 1.11 shows a schematic of the test piles. The 20 in. × 20 in. × 516 in. square pile was prestressed using fourteen 0.5 in. diameter seven-wired strands of prestressing steel with an ultimate strength of 270 ksi, and pretensioned to produce a prestress level of 0.809 ksi. Lateral reinforcement was provided by a No. 5 gauge spiral wire. The specified compressive strength of concrete was 5.8 ksi. The circular precast composite pile consists of a GFRP tube, with an outer diameter of 24.6 in. and a structural wall thickness of 0.213 in., filled with concrete with shrinkage reducing admixture. Specified compressive strength of concrete was 6 ksi. The composite pile had a length of 516 in. Both piles were instrumented as shown in Figure 1.12. Based on the compressive strengths of concrete for the piles, and the properties of steel reinforcement and the GFRP tubes, the estimated axial load capacities of the prestressed and composite piles are 2071 kips and 2812 kips respectively.

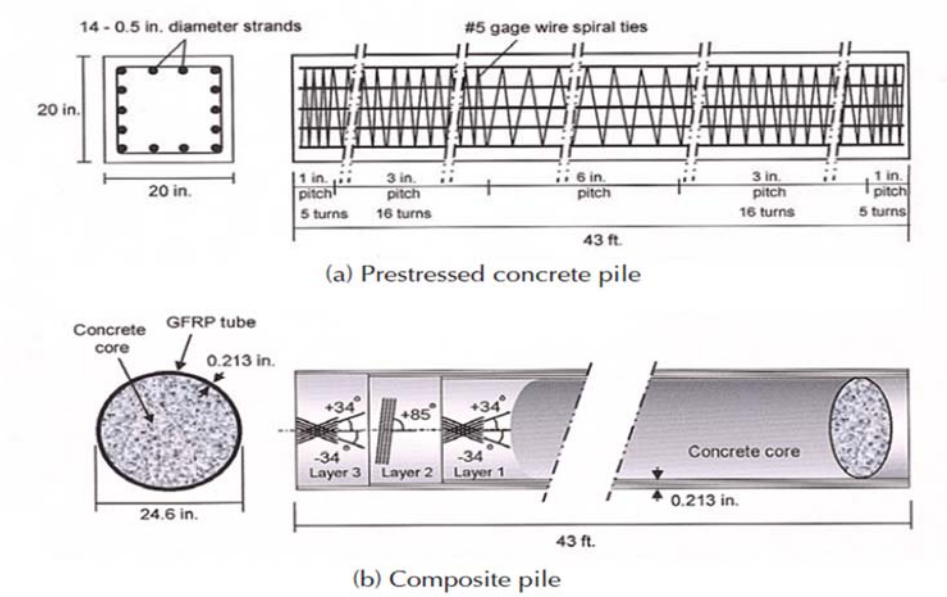

Figure 1.11: Pile details (Fam et al., 2003)

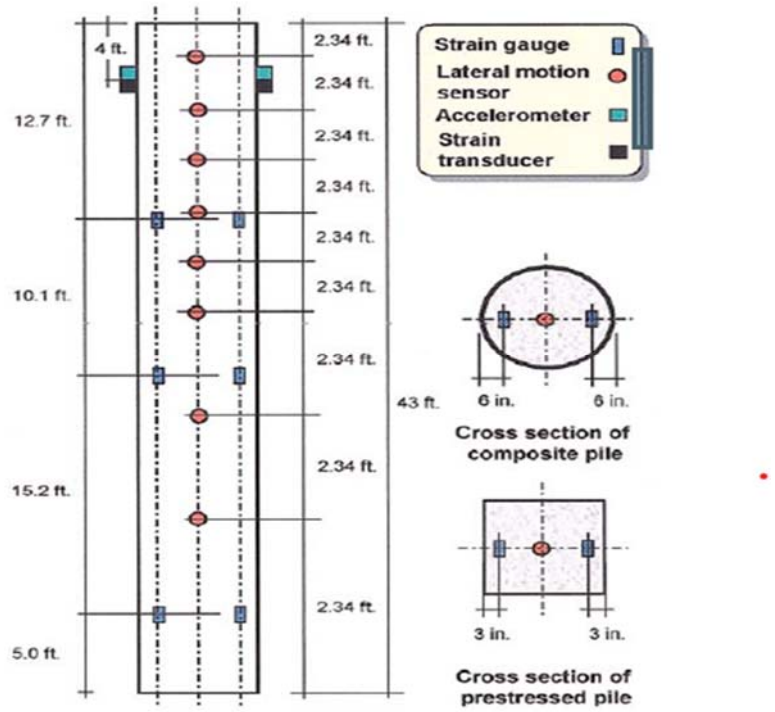

Figure 1.12: Instrumentation of test piles (Fam et al., 2003)

Both piles were driven with an ICE Model 160S hydraulic impact hammer with a ram weight of 16,000 lbs. To avoid damaging the pile head due to the high impact mass, a plywood cushion with a thickness of 7.5 in. was used. The piles were driven to 33.5 ft below ground level. Blow counts during driving were four blows per inch for the prestressed concrete pile and six blows per inch for the composite pile. Information on the surrounding soil properties were not provided.

Measurements obtained for the prestressed pile during driving indicated a wave speed of 12,150 ft/s. Maximum compressive strength and maximum tensile stress were 2.55 ksi and 0.75 ksi respectively, which were well within the allowable stress of 4.5 ksi in compression and 1.02 ksi in tension. The composite pile measurements on the other hand, indicated a wave speed of 11,840 ft/s. Maximum compressive strength and maximum tensile stress were 2.78 ksi and 0.42 ksi respectively. The results showed that the driving performance of the piles were relatively similar.

Research performed by **Rausche et al. (2008)** to investigate the relationship between ram weight, penetration of pile into soil, and stresses in a series of pile types, indicated that compression stresses in piles are dependent primarily on ram weight and cushion properties. A heavy ram reduced tension stresses which may occur due to a very low resistance. The square prestressed concrete pile tested had a length of 85.58 ft (27 m), a cross-sectional area of 387.50 in^2 (0.25 m^2) and a weight of 35.74 kips (158 kN). The ram – pile weight ratio for the test was 0.94. Results obtained for the pile indicated a tension stress of 0.52 ksi (3.6 Mpa) and a compression stress of 3.62 ksi (25 Mpa).

Roddenberry et al. (2014) drove two 24 in. square CFRP prestressed concrete piles to refusal as part of the Deer Crossing Bridge project. Both piles were 100 ft in length and were reinforced longitudinally with twenty 0.6 in. diameter CFRP prestressing strands. The diameter of the CFRP spirals were 0.2 in. The first pile was driven normally at the initial driving stage before being subjected to hard driving at the latter stage of the driving the pile. The second pile was subjected to hard driving during the entire installation process to further test the limits of the pile. Stresses in both piles were measured by Embedded Data Collectors (EDC) – strain transducers and accelerometers embedded in the pile, and the Pile Driving Analyzer which uses accelerometers and strain transducers attached to the surface of the piles to measure forces and velocities. As discussed in section 1.5, the measured stress was up to 4.0 ksi, which was smaller than the maximum allowed pile compressive stress of 6.25 ksi (based on the measured compressive strength $f_c' = 10000$ and design $f_{pe} = 1000$). The maximum allowable pile stress was determined according to equations in Florida DOT Standard Specifications 455-5.12.2 (FDOT, 2018). Detailed measurement obtained from driving both piles can be found in Appendix E of the report by Roddenberry et al. (2014).

BIBLIOGRAPHY

Ashford, S. A. and Jakrapiyanun, W. (2001). "Drivability of glass FRP composite piling." *Journal of Composites for Construction*, *5*(1), 58–60.

Bullock, P.J. (1999). "Pile friction freeze: A field and laboratory study." Ph.D. Dissertation. Department of Civil Engineering. University of Florida. Gainesville, FL.

Bullock, P. J. (2008). "The easy button for driven pile setup: Dynamic testing." *From Research to Practice in Geotechnical Engineering*, 471–488.

Bullock, P. J. (2012). "Advantages of dynamic pile testing." *Full-Scale Testing and Foundation Design: Honoring Bengt H. Fellenius*, 694–709.

Bullock, P. J., Schmertmann, J. H., McVay, M. C., and Townsend, F. C. (2005). "Side shear setup. I: Test piles driven in Florida." *Journal of Geotechnical and Geoenvironmental Engineering*, *131*(3), 292–300.

Consolazio, G. R., Bui, L. H., and Walters, R. A. (2012). "Pendulum impact testing of an impact-breakaway, wind-resistant base connection for multi-post ground signs." *Structures Research Rep. No. 2012/92174*, University of Florida

Consolazio, G. R., Getter, D. J., and Kantrales, G. C. (2014). Validation and Implementation of Bridge Design Specifications for Barge Impact Loading, *Structures Research Rep. No*. 2014/87294, University of Florida

Clough, R. W. and Penzien, J. (1993). *Dynamics of structures.* Berkeley, CA: Computers and Structures, Inc.

Ding, X., Liu, H., Liu, J., and Chen, Y. (2011). "Wave propagation in a pipe pile for low-strain integrity testing." *Journal of Engineering Mechanics*, *137*(9), 598–609.

El-Garhy, B., Galil, A. A., Youssef, A.-F., and Raia, M. A. (2013). "Behavior of raft on settlement reducing piles: Experimental model study." *Journal of Rock Mechanics and Geotechnical Engineering*, *5*(5), 389– 399.

Fam, A., Pando, M., Filz, G., and Rizkalla, S. (2003). "Precast piles for Route 40 bridge in Virginia using concrete-filled FRP tubes." PCI J., 48(3), 32–45

FDOT (2018). *FDOT Standard Specifications for Road and Bridge Construction*.Florida Department of Transportation, Tallahassee, FL.

Florida Department of Transportation (2015). *Pile Driving Inspectors Qualification Course*. Florida Department of Transportation.

Guades, E., Aravinthan, T., Islam, M., and Manalo, A. (2012). "A review on the driving performance of FRP composite piles." *Composite Structures*, *94*(6), 1932 – 1942.

Hannigan, P. J., Rausche, F., Likins, G. E., Robinson, B. R., and Becker, M. L. (2016a). "*Design and construction of driven pile foundations-volume I*" Report no., Federal Highway Administration.

Hannigan, P. J., Rausche, F., Likins, G. E., Robinson, B. R., and Becker, M. L. (2016b). "*Design and construction of driven pile foundations-volume II*." Report no., Federal Highway Administration.

Herrera, R., Jones, L. E., and Lai, P. (2009). "Driven concrete pile foundation monitoring with embedded data collector system." *Contemporary Topics in Deep Foundations*, 621–628.

Herrera, R., Jones, L.E., Kim, M., (2018) "Relaxation of Displacement Driven Pile Foundations in Florida's Granular Soils" ASCE (G-I) Geotechnical Special Publication No. 294, pp. 201 to 210. *Proceedings of the International Foundations Congress and Equipment Expo 2018*

Hussein, M. H. and Goble, G. G. (2004). "A brief history of the application of stress-wave theory to piles." *Current Practices and Future Trends in Deep Foundations*, 186–201.

Hussein, M. H., Woerner, II, W. A., Sharp, M., and Hwang, C. (2006). "Pile driveability and bearing capacity in high-rebound soils." *GeoCongress 2006: Geotechnical Engineering in the Information Technology Age*, 1–4.

Kantrales, G. C., Consolazio, G. R., Wagner, D., and Fallaha, S. (2015). "Experimental and analytical study of high-level barge deformation for barge–bridge collision design." *Journal of Bridge Engineering*, *21*(2), 04015039.

Likins, G. (1984). "Field measurements and the pile driving analyzer." *Proceedings of the Second Interna- tionalConference on the Application of Stress-Wave Theory on Piles, Stockholm*, 298–305.

McVay, M., Bloomquist, D., Vanderlinde, D., and Clausen, J. (1994). "Centrifuge modeling of laterally loaded pile groups in sands." *Geotechnical Testing Journal*, *17*(2), 129–137.

McVay, M., Zhang, L., Molnit, T., and Lai, P. (1998). "Centrifuge testing of large laterally loaded pile groups in sands." Journal of Geotechnical and Geoenvironmental Engineering, 124(10), 1016–1026.

McVay, M. C., Alvarez, V., Zhang, L., Perez, A., and Gibsen, A. (2002). "Estimating driven pile capacities during construction." Report no. WPI 0510852.

McVay, M. C., Wasman, S. J., et al. (2015). "*Embedded data collector (EDC) phase ii load and resistance factor design (LRFD).*" Report no., Florida. Dept. of Transportation.

McVay, M. C., Zhang, L., Han, S., and Lai, P. (2000). "Experimental and numerical study of laterally loaded pile groups with pile caps at variable elevations." *Transportation research record*, *1736*(1), 12–18.

Rausche, F., Hussein, M., Likins, G., and Thendean, G. (1994). "Static pile load-movement from dynamic measurements." *Vertical and Horizontal Deformations of Foundations and Embankments*, ASCE. 291–302.

Rausche, F. (2000). "Pile driving equipment: Capabilities and properties." *Keynote lecture, Proceedings of the 6th International Conference on the Application of Stress-Wave Theory to Piles, Rotterdam.*

Rausche, F., Likins, G., Miyasaka, T., & Bullock, P. (2008). *The effect of ram mass on pile stresses and pile penetration.* Paper presented at the The 8 th international conference on the application of stress wave theory to piles, Science, Technology and Practice.

Rausche, F., Likins, G., Liang, L., and Hussein, M. (2010). "Static and dynamic models for capwap signal matching." *Art of foundation engineering practice*, 534–553.

Roddenberry, M., Mtenga, P., and Joshi, K. (2014). "Investigation of Carbon Fiber Composite Cables (CFCC) in Prestressed Concrete Piles," Florida Department of Transportation Final Report, BDK83-977-17.